Lithium conducting solid electrolyte $Li_{1.3}Al_{0.3}Ti_{1.7}(PO_4)_3$ obtained via solution chemistry

Sandrine Duluard [a,*], Aude Paillassa [a], Laurent Puech [b], Philippe Vinatier [b], Viviane Turq [a], Patrick Rozier [a], Pascal Lenormand [a], Pierre-Louis Taberna [a], Patrice Simon [a], Florence Ansart [a]

[a] *Institut Carnot CIRIMAT (CNRS/Université Paul Sabatier - UMR 5085), 118 route de Narbonne, F-31602 Toulouse Cedex 9, France*
[b] *ICMCB, CNRS, Université de Bordeaux, site de l'ENSCBP-IPB (CNRS - UPR9048), 87 avenue du Dr. Schweitzer, F-33608 Pessac, France*

Abstract

NaSICON-type lithium conductor $Li_{1.3}Al_{0.3}Ti_{1.7}(PO_4)_3$ (LATP) is synthesized with controlled grain size and composition using solution chemistry. After thermal treatment at 850 °C, sub-micronic crystallized powders with high purity are obtained. They are converted into ceramic through Spark Plasma Sintering at 850–1000 °C. By varying the processing parameters, pellet with conductivities up to 1.6×10^{-4} S/cm with density of 97% of the theoretical density have been obtained. XRD, FEG-SEM, ac-impedance and Vickers indentation were used to characterize the products. The influence of sintering parameters on pellet composition, microstructure and conductivity is discussed in addition to the analysis of the mechanical behavior of the grains interfaces.

Keywords: Powders-chemical preparation; Sintering; Microstructure; Ionic conductivity; Batteries

1. Introduction

Batteries are key systems for the development of technologies such as portable devices and transportation systems. One of the most appealing challenges is the increase of their specific mass energy for applications requiring large energy storage capacity e.g. electric vehicle or grid storage.[1,2] In this respect, reversible lithium-air batteries with an expected energy density of more than 500 Wh/kg i.e. a potential range of more than 800 km have shown promising results.[3–5] So far, two main solvent-based technologies have been studied: aqueous[6,7] and non aqueous lithium-air devices.[8,9] Other concepts are also being investigated, e.g. an all-solid state device was described recently by Kumar et al.[10] In water-based devices, the main electrolyte is aqueous-saturated lithia. In order to prevent reactions of the lithium anode with the aqueous electrolyte, an ionic conducting separator is necessary. Accordingly, a lithium-conducting solid electrolyte is necessary for both all-solid state and water-based technologies. Solid electrolytes such as Li_3N compounds and sulfide-based glasses are good candidates with conductivity as high as 6×10^{-3} S/cm.[11] However, being hygroscopic, their fabrication in inert atmosphere is mandatory. Oxide electrolytes such as LiSICON electrolyte are more suited due to their ease of preparation. Even though LiSICON type compound $Li_{2+2x}Zn_{1-x}GeO_4$ ($0.45 < x < 0.55$) was reported as being highly conductive, its conductivity is still too low at room temperature (10^{-6} S/cm).[12] With conductivity in the range of 10^{-4} S/cm, NaSICON type $Li_{1+x}Al_xTi_{2-x}(PO_4)_3$ (LATP) compounds with $x = 0.3$–0.4 benefit from one of the best lithium conductivity amongst air and moisture stable compounds.[13] In strongly reducing environment (e.g. lithium metal electrode), LATP materials are combined with a protective layer (e.g. LiPON) to avoid Ti^{4+} reduction.[14] The synthesis of LATP via solid-state chemistry is much documented.[15,16] Thanks to the large choice in the raw material nature and synthesis parameters, solution chemistry favors the preparation of powders with controlled composition and morphology. In this work, we propose a method for the preparation of high-purity LATP powder by co-precipitation. By optimization of the sintering parameters, pellets with conductivity as high as 1.6×10^{-4} S/cm at room temperature were prepared.

* Corresponding author. Tel.: +33 5 61 55 72 92; fax: +33 5 61 55 61 63.
E-mail address: duluard@chimie.ups-tlse.fr (S. Duluard).

http://dx.doi.org/10.1016/j.jeurceramsoc.2012.08.005

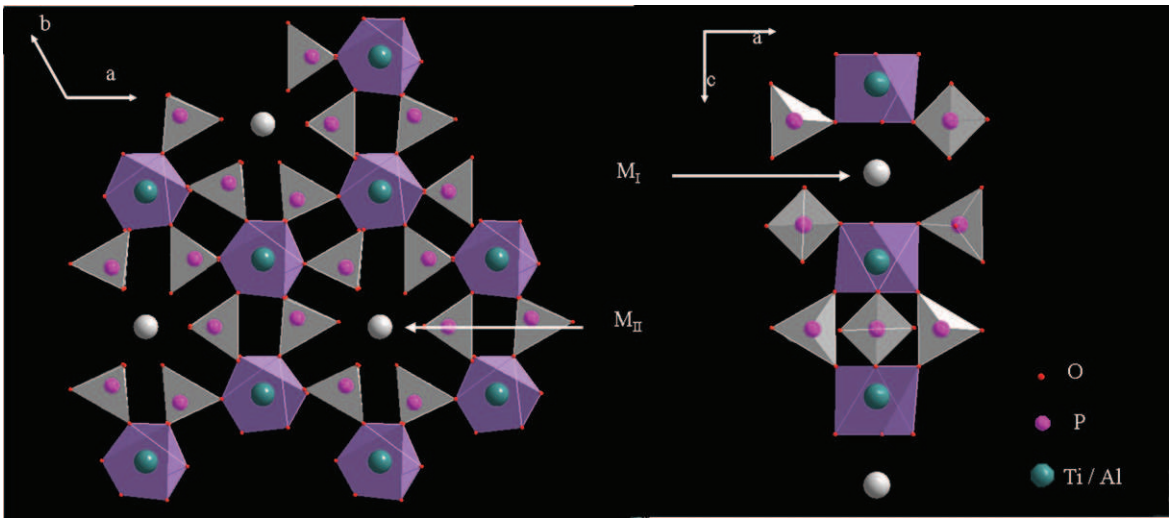

Fig. 1. Projection of the structure of $Li_{1+x}Al_xTi_{2-x}(PO_4)_3$. The M_I and M_{II} intercalation sites correspond respectively to the main occupied and excess (x) Li^+ sites.

2. Experimental

Crystallographic phases analysis was carried out by X-ray diffraction with a Brucker D4 Endeavor diffractometer using a Cu Kα radiation source (Kα = 0.15418 nm). Elementary analyses were performed by SCA – CNRS. Inductively couple plasma (ICP) analyses were used for quantity determination of lithium, aluminium, titanium and phosphorus. Thermogravimetric analyses were performed on a Setaram TG-DTA 92 microbalance with 30 mg of sample and alumina as a reference. Scanning electron microscope with Field Emission Gun (FEG-SEM) JEOL JSM 6700F with a 5 kV accelerating voltage was used for morphological and microstructural investigations. Agglomerates sizes were determined by laser granulometry. The density of the pellets was determined via Archimede's method on a KERN ARJ 220-4 M balance. A density of 2.92 g/cm^3 is taken as the theoretical value of bulk LATP ($x = 0.3$). Surface roughness of the pellets was studied by optical surface profilometry with an optical interferometer Zygo New View 100 with MetroProTM software. Impedance spectroscopy was used to determine the conductivity of the pellets. Gold electrodes were deposited on the two faces of the pellets by a gold sputter-coater. Impedance measurements at frequencies from 1 Hz to 10^7 Hz with varying temperature were performed using a Solartron 1260 impedance analyser and a furnace equipped with a Eurotherm temperature controller. Micro hardness tests were performed on a polished surface with a Vickers indenter HMV-2000 Shimadzu.

3. LATP powders synthesis and characterization

The powder synthesis is based on the co-precipitation of alkoxide and metallic salts adapted from a procedure of Cretin et al.[17] The water/ethanol ratio, hydrolysis ratio and annealing temperature were optimized.

3.1. LATP powder synthesis

Li acetate dihydrate ($CH_3CO_2Li{\cdot}2H_2O$, ≥99%), ammonium phosphate monobasic ($NH_4H_2PO_4$, 99.999% pure), aluminium tri-sec butoxide (Al(tri-sec-OBu), ≥97%) and titanium isopropoxide ($Ti(OiPr)_4$, ≥97%) were used as raw precursors and purchased from Sigma–Aldrich. A solution v/v 80/20 water/ethanol with a concentration of 0.4 mol/L of metallic salts and stoichiometric proportions of precursors is obtained by addition of a water based solution with appropriate amounts of lithium acetate and ammonium phosphate monobasic in the ethanol solution containing titanium and aluminium alkoxides. The hydrolysis ratio ($h = [H_2O]/([Ti(OiPr)_4] + [Al(tri\text{-}sec\text{-}OBu)]$) was high ($h = 200$), so that polycondensation occurred and a precipitate was formed. Solution was stirred for 2 h at room temperature. After solvent evaporation at 80 °C for 48 h a white powder was obtained. The resulting powder was annealed at temperature from 450 °C to 1100 °C for 150 min with a 100 °C/h temperature ramp in heating and 300 °C/h in cooling.

3.2. Structure description and phase analysis

$Li_{1+x}Al_xTi_{2-x}(PO_4)_3$ (LATP, $x = 0$–0.5) belongs to the NaSICON-type ($Na_{1+x}Zr_2Si_xP_{3-x}O_{12}$, $0 < x < 3$) structure. It crystallizes in the rhombohedral system (space group $R3\bar{c}$) with cell parameters $a = 8.48(2)$ Å, $c = 20.76(2)$ Å.[16] The structure is built up with TiO_6 octahedra and PO_4 tetrahedra sharing corners to form a 3-D open framework as schematized in Fig. 1. Li cations are located into two sites labeled M_I and M_{II}. The main one (M_I), which is identical to that of un-substituted LTP parent structure, corresponds to a distorted octahedral oxygenated environment. The substitution of Al^{3+} to Ti^{4+} leads, for charge compensation, to extra lithium ions located in M_{II} sites with irregular eight coordinated sites.[18,19]

By analogy with NaSICON, the migration pathway of Li^+ ions in LTP is speculated to occur via bottlenecks along a path

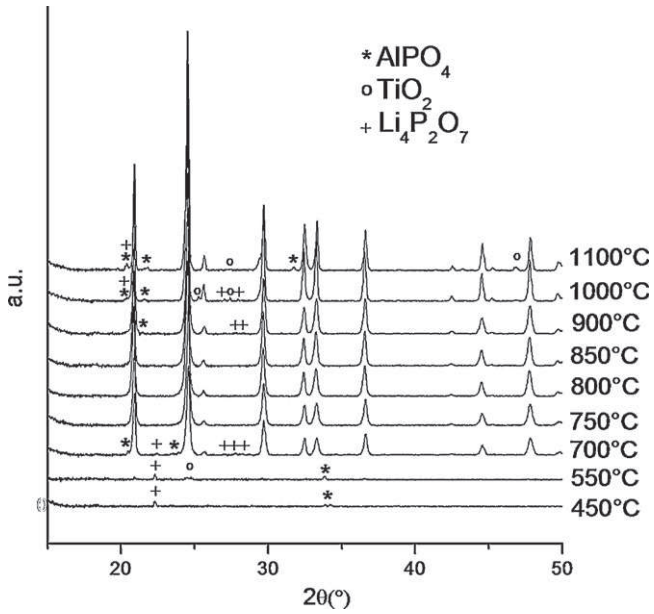

Fig. 2. X-ray diffraction diagrams measured at room temperature for LATP powder annealed at temperature from 450 °C to 1100 °C.

M_I-M_{II}-M_I.[19,20] It was also shown that the narrowest places of the bottleneck shaped channel are large enough for Li^+ ion to migrate without any distortion of the LTP network. Ti^{IV} substitution by Al^{III} contributes to open the bottleneck size by increasing the occupation of the M_{II} sites.[21] This effect added to the increase in Li^+ concentration favors Li^+ diffusion in LATP as compared to LTP. This results in conductivity at room temperature of 10^{-4} S/cm for LATP for $x = 0.3$–0.4 versus 2×10^{-6} S/cm for LTP.[22]

X-ray diffraction patterns of samples annealed at temperature ranging from 450 °C to 1100 °C are reported in Fig. 2. The crystallization of LATP occurs at 700 °C. Pure LATP is obtained for annealing temperatures from 750 °C to 850 °C. Above 850 °C, decomposition occurs leading to the formation of secondary phases $AlPO_4$, TiO_2 and $Li_4P_2O_7$. For further experiments, the annealing temperature is then set at 850 °C.

The composition of this powder was checked by inductively coupled plasma (ICP) elementary analyses. A composition of $Li_{1.21\pm0.01}Al_{0.32}Ti_{1.72\pm0.02}P_3O_{12}$ was then obtained which implies an evaporation of 0.2% w/w of lithium as compared to the theoretical stoichiometry $Li_{1+x}Al_xTi_{2-x}(PO_4)_3$ with $x = 0.3$. This corresponds to a maximum of 2–4 w/w % of impurities ($AlPO_4$ or $Li_4P_2O_7$ by-product considered) present in the powder.

3.3. Powder morphology

Scanning electron micrographs of LATP powder are presented in Fig. 3. The non annealed powder is mostly composed of particles of 50–100 nm in size with additional larger particles of 200–400 nm. The annealing at 850 °C leads to particles larger than 100 nm with a large distribution in shapes. The results of the 850 °C annealed powder are confirmed by laser granulometry, as presented in Fig. 3(b), with a calculated mean

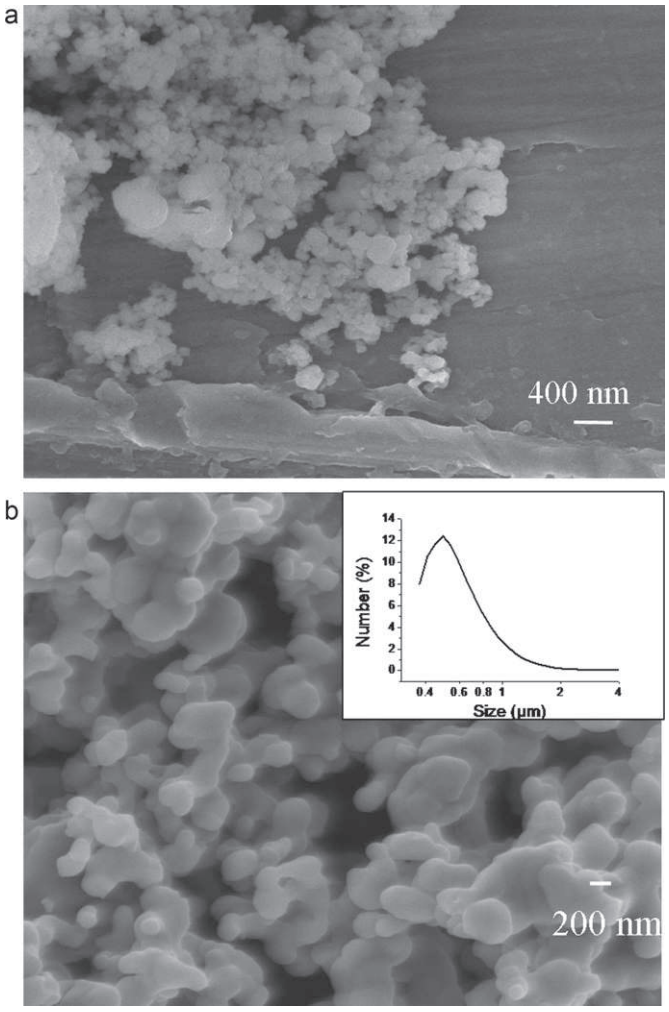

Fig. 3. Images of LATP powder obtained by scanning electron microscopy and distribution in size of particles obtained by laser granulometry: (a) powder before thermal treatment, (b) powder annealed at 850 °C.

diameter of 520 nm and 90% of the agglomerates in the range of 400–1000 nm.

3.4. Powder conductivity

To our knowledge, whereas LATP structure with $x = 0.3$ has been demonstrated as convenient for lithium conduction, no mention of the percolation behavior of such powder has been reported in the literature. In order to determine whether a percolation network could be formed at room temperature between the LATP grains, the conductivity of a pressed pellet has been measured by impedance spectroscopy. The chosen LATP powder (annealed 850 °C, 2 h 30) was pressed in between two brass disc electrodes. The maximum compaction, which corresponds to the minimum in sample thickness, is reached at an applied pressure of 110 MPa. Nyquist impedance plots for several applied pressure present the same behavior. One semicircle is observed at high frequency and an inclined tail is observed at low frequencies. The resistance was measured by fitting the semi-circle plot using a conventional equivalent circuit

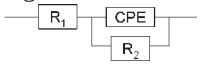

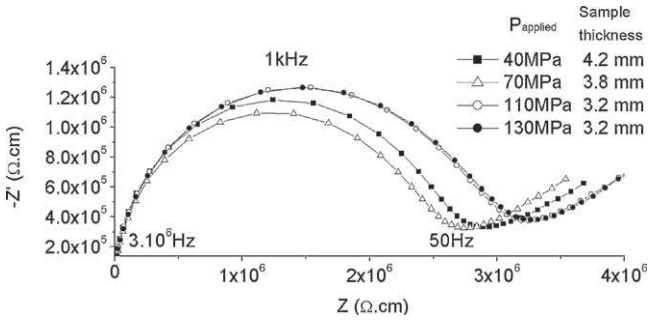

Fig. 4. Impedance spectra of the pressed powder depending on the pressure applied and corresponding conductivity.

with R_1 the electrical resistance of the measurement system, R_2 the resistance of the electrolyte and CPE the corresponding constant phase element.[23] The Nyquist plots normalized in surface and thickness are given in Fig. 4(a). No difference of resistivity is measured as compaction increases and thickness decreases so that the measured phenomenon arises directly from the resistance being proportional to the pellet thickness. Whatever the compaction ratio, a low conductivity (in the range of $3.1–3.6 \times 10^{-7}$ S/cm) is obtained. The contact between the grains is not efficient enough to create a percolation network that would enhance lithium conductivity.

4. Ceramic sintering

Since physical binding is not sufficient enough for allowing lithium conduction within the pellets, sintering of the powder was performed to promote chemical bonding between the grains. LATP powders annealed at 850 °C were pressed into pellets between two sheets of graphite papers (Papyex®) and sintered under vacuum using the Spark Plasma Sintering (SPS) technique in a SPS 2080 Sumitomo apparatus. A pulse sequence (12 pulses, 2 idle time, 3.3 ms/cycle) with adjusted current was applied. The die was heated up to the sintering temperature with a 100 °C/min ramp. An isostatic pressure of 100 MPa was applied before heating. The beginning of the sintering occurs at 750 °C with a maximum in the shrinkage rate at 800–850 °C as observed by dilatometric studies.

4.1. Sintered pellets and processing parameters

A summary of the various sintering conditions is indicated in Table 1. Temperature from 850 °C to 1000 °C and duration from 5 min to 20 min were used. After sintering, the samples were polished in order to remove the graphite paper.

Table 1
Sintering conditions for the preparation of pellets.

Ceramic pellets	Sintering temperature (°C)	Sintering duration (min)
A1-850-5	850	5
B1-900-5	900	5
C1-950-5	950	5
D1-1000-5	1000	5
A2-850-10	850	10
A3-850-15	850	15
A4-850-20	850	20

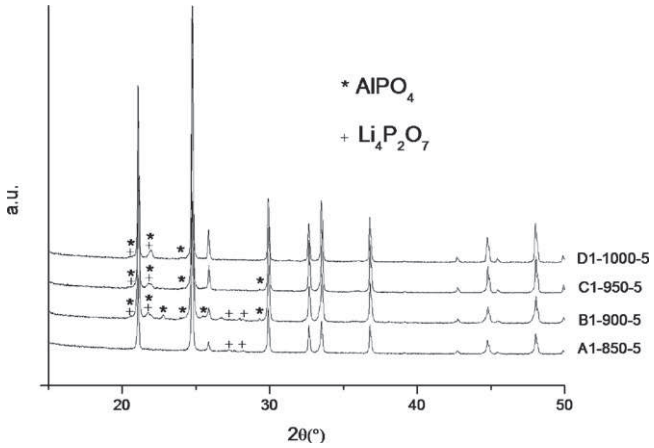

Fig. 5. X-ray diffraction diagrams at room temperature for pellets sintered by SPS under 100 MPa applied pressure, vacuum atmosphere. Sintering duration: 5 min. Sintering temperatures: 850 °C, 900 °C, 950 °C, 1000 °C.

4.2. Crystallographic phases analysis of the pellets

XRD patterns for the sintered pellets versus the sintering temperature and sintering duration are presented in Figs. 5 and 6. All the major peaks are indexed in the crystal system of the LATP powder. No change in cell parameters is observed ($a = 8.48 \pm 0.02$ Å and $c = 20.76 \pm 0.03$ Å). Side products $AlPO_4$ appear in all the pellets, except for the pellet sintered at the lowest temperature for short time (850 °C, 5 min) in which only a small amount of $Li_4P_2O_7$ is present. $Li_4P_2O_7$ could be present in all the samples, however in some cases only the major peak ($2\theta = 20.5°$) that is a common peak with $AlPO_4$ phases is visible. In addition, a Li_2C_2 phase is detected for pellets sintered for more than 5 min. A sharpening of the peaks on the XRD patterns is observed for sintering temperature from 850 °C to 950 °C, so that the primary particles increase in size with increasing sintering temperature.

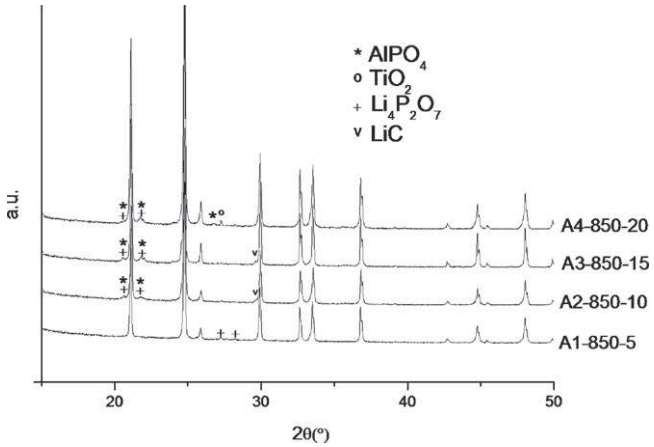

Fig. 6. X-ray diffraction diagrams at room temperature for pellets sintered by SPS under 100 MPa applied pressure, vacuum atmosphere. Sintering temperature: 850 °C. Sintering duration: 5, 10, 15, 20 min.

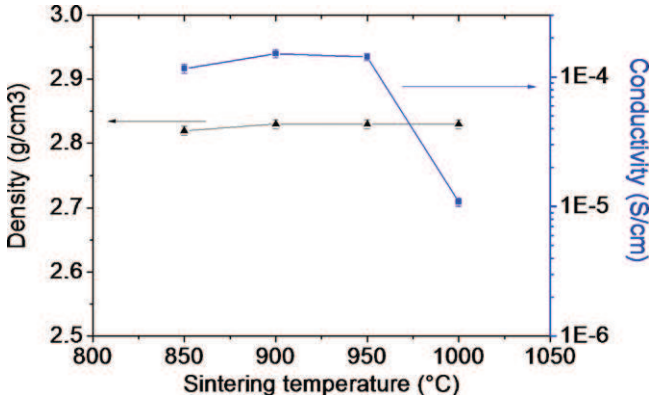

Fig. 7. Density measured by Archimede's method and conductivity measured by electrochemical impedance spectroscopy. Pellets A1-850-5, B1-900-5, C1-950-5, D1-1000-5. Duration of sintering: 5 min.

5. Results and discussions

5.1. Density and conductivity

Figs. 7 and 8 show the evolution of the density (measured at room temperature) of the SPS-prepared pellets versus sintering temperature and duration. Whatever the sintering conditions, pellets with density ranging from 2.82 g/cm^3 to 2.84 g/cm^3 (i.e. 97% of the theoretical density) were obtained. It should be noted that since all the samples have the same density, the direct comparison of the conductivity of the LATP pellets is accurate.

Room temperature conductivities of the pellets exhibit a similar behavior to the one described for LATP powder in Section 3.4. Only one semi-circle, representative of the total resistance of the electrolyte, is observed. Values from 1×10^{-4} S/cm to 1.6×10^{-4} S/cm are obtained for pellets sintered between 850 °C and 950 °C. These values, similar to those reported in the literature,[1,3,24] indicate in addition that the conductivity increases with increasing temperatures. However, while sintering at temperature above 1000 °C leads to almost fully dense pellets, their conductivities drop down to 1×10^{-5} S/cm which fully contradict the expected evolution.

The effect of sintering duration has also been studied and plotted in Fig. 8 for a sintering temperature of 850 °C. The densities and conductivities remain the same independent of the duration of sintering from 5 min to 20 min. Then, the secondary phase formation detected by XRD (cf. Section 4.2) on the sample sintered at 10–20 min is not detrimental to density and conductivity.

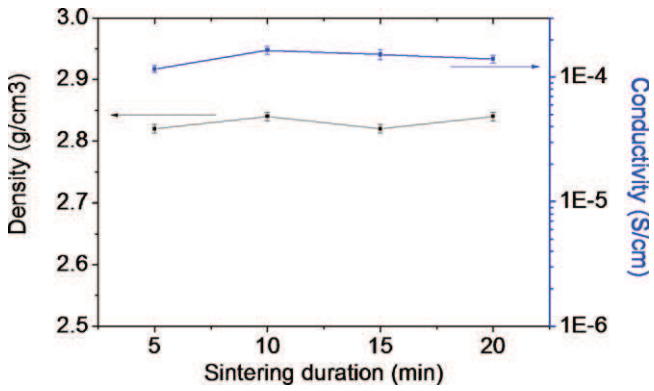

Fig. 8. Density measured by Archimede's method and conductivity measured by electrochemical impedance spectroscopy. Pellets A1-850-5, A2-850-10, A3-850-15, A4-850-20. Temperature of sintering: 850 °C.

5.2. Microstructural analysis of the pellets

In order to determine whether the difference in conductivity could be related to a change in microstructure, SEM micrographs analysis of the cross-section of the samples has been performed. The microstructure of the pellets strongly depends on the sintering temperature. Whereas the pellet sintered at 1000 °C present a uniform microstructure with large grains (6–30 μm in diameter), for pellets sintered at 850 °C and up to 950 °C, a heterogeneous microstructure appears. As presented in Fig. 9, parts with only small grains of 200–300 nm in diameter were present close to zones with large grains of tens of micrometres. As temperature increases, the surface area covered by large grains becomes predominant. On the contrary, the duration of sintering does not mainly influence the microstructure. The same structure with large and small grains is obtained for pellets sintered at 850 °C for 5, 10, 15 and 20 min (micrographs not shown here). For LATP materials ($x = 0.3$–0.4), bulk conductivity is reported to be higher than grain boundaries conductivity.[17] The presence of larger grains is then expected to be beneficial to conductivity which fully agrees with the observed evolution for pellets sintered between 850 °C and 950 °C. However, the drop down in conductivity observed at 1000 °C, whereas only a population of large grains is observed, contradicts this expected evolution. The aggregation of a non Li^+ conductive secondary phase at the grain boundaries could explain this phenomenon. However no significant difference in grain boundaries compositions has been observed by EDX analyses on conductive and non conductive samples. A careful observation of pellets sintered above 1000 °C indicates that the cohesion between large grains is weak as shown in Fig. 10. Then the lack of cohesion between the grains can be suspected to be at the origin of the drop in conductivity.

5.3. Mechanical properties

In order to study the mechanical behavior of the zones with small grains and the zones with large grains, Vickers microhardness measurements under various normal loads (2 N, 2.9 N, 4.9 N and 9.8 N) were performed. Optical microscopy and SEM analyses of the indented surfaces have been carried out.

A Vickers hardness decrease from 700–800 HV for the zones with small grains to only 300–400 HV in the zones consisting of large grains is observed. The decrease of plastic yield stress with increasing grain size has been described by the Hall–Petch law: $\sigma_y = \sigma_\infty + kd^{-1/2}$, with d the grain size, k a constant, σ_∞ yield stress of the single crystal, σ_y plastic yield stress that is considered as proportional to the hardness for such ceramics.[25]

This law is relevant for grains from several tens of nanometers to several tens of microns such as the size of grains in the materials studied in this work. Moreover, fractures surging from the sides of the Vickers indentation are only visible in

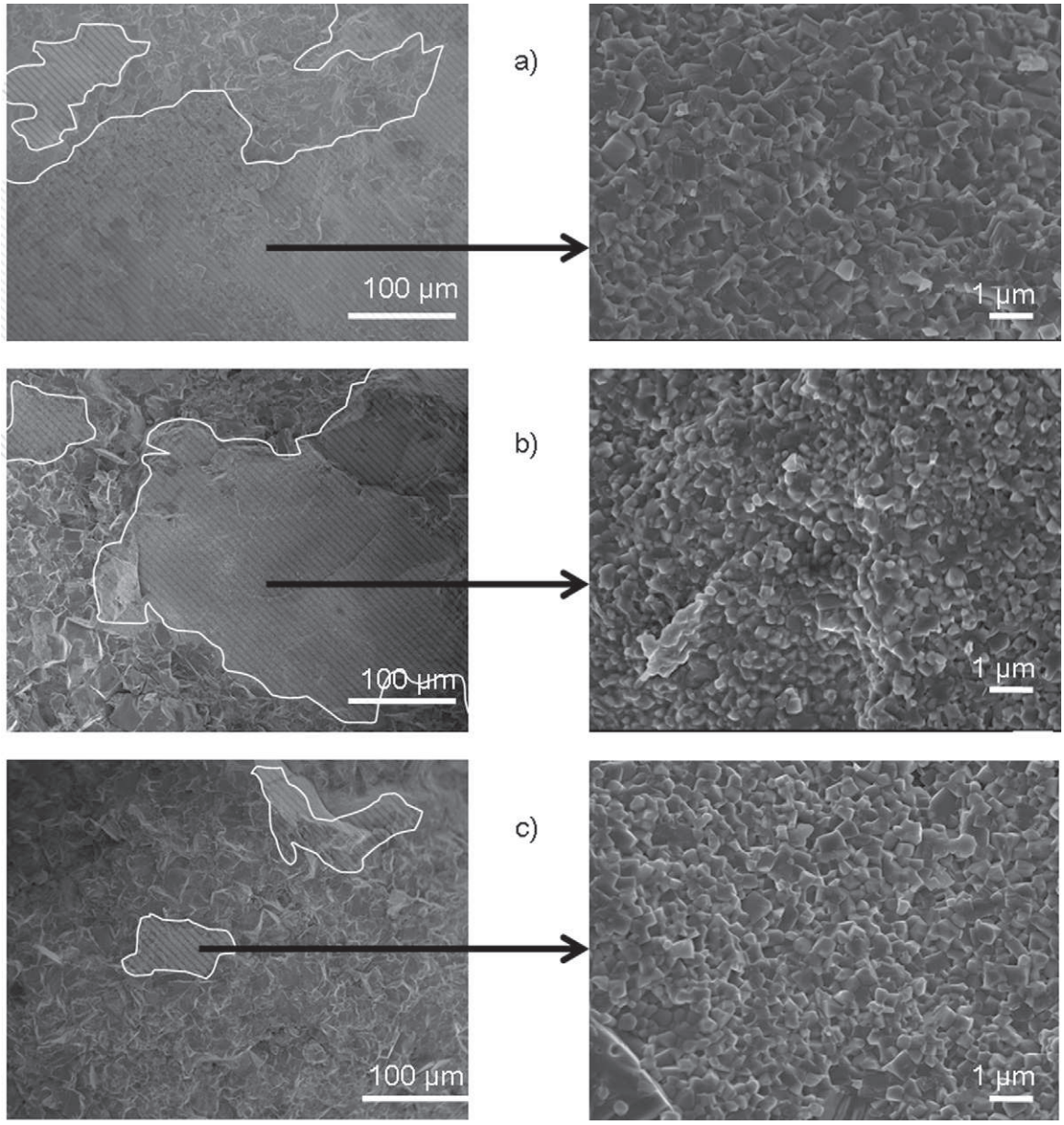

Fig. 9. SEM images of the fracture surface of pellets sintered at (a) 850 °C, (b) 900 °C and (c) 950 °C.

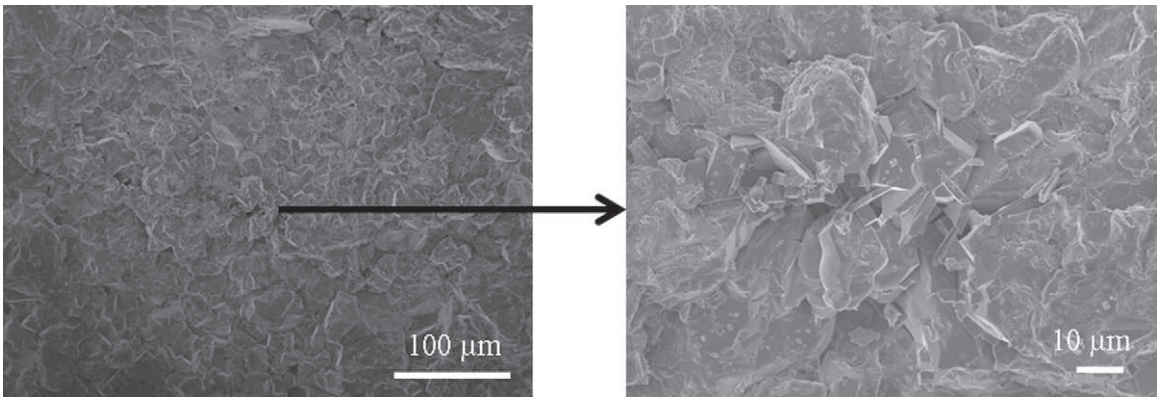

Fig. 10. SEM images of the fracture surface of pellets sintered at 1000 °C.

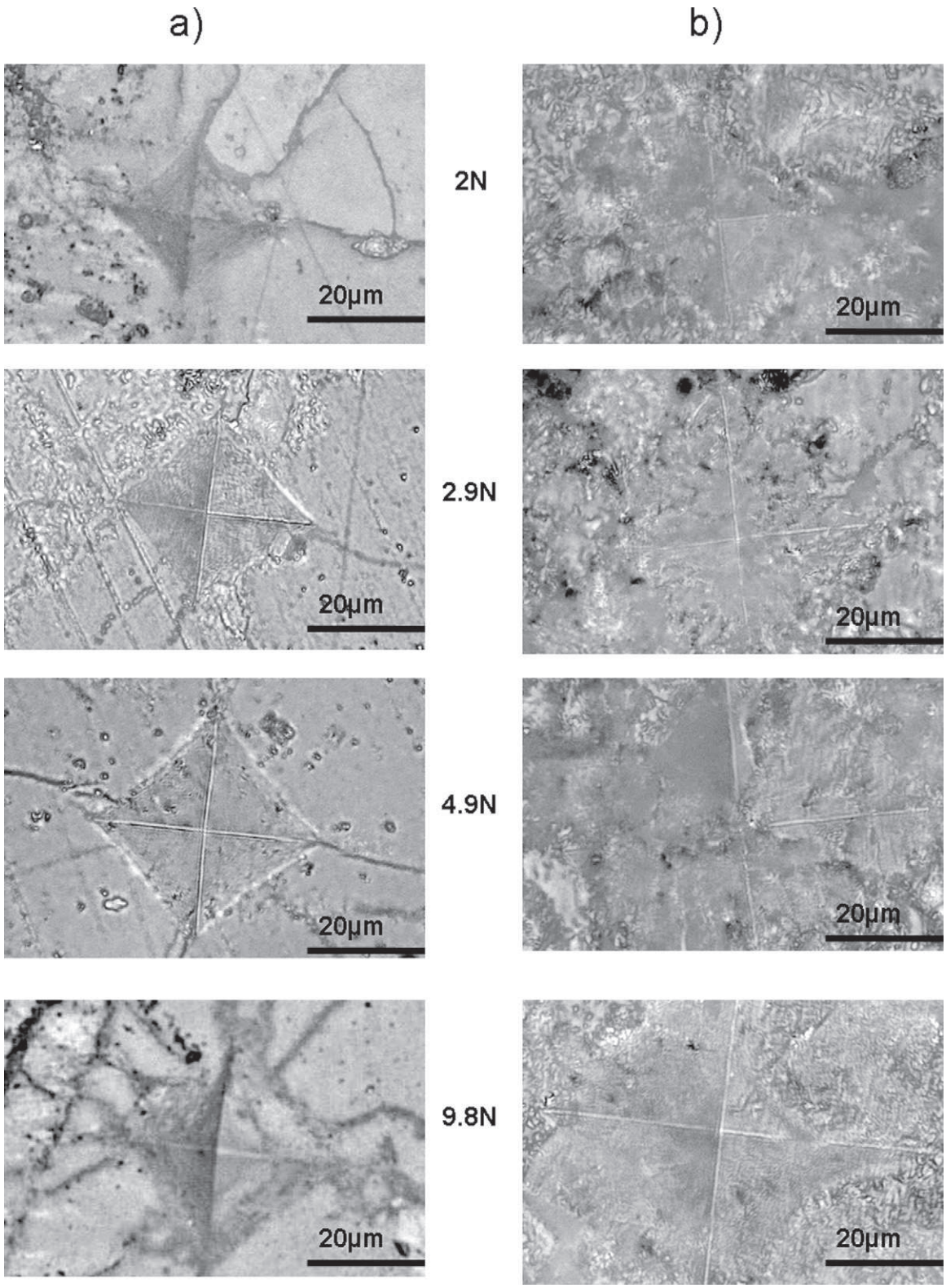

Fig. 11. Optical micrographs of Vickers hardness indentation marks in sintered pellets for several applied loads. (a) Zones with small grains and (b) zones with large grains.

the zones with small grains due to the higher hardness of this zone.

Optical micrographs after indentation on zones with large grains and zones with small grains are shown in Fig. 11. A deformation around the indentation is visible in both cases even for the lowest load (2 N). The zones with large grains are more subject to large deformations at the edge of the indentation. Under a load from 2 N to 9.8 N, the mark left in this zone is 1.5

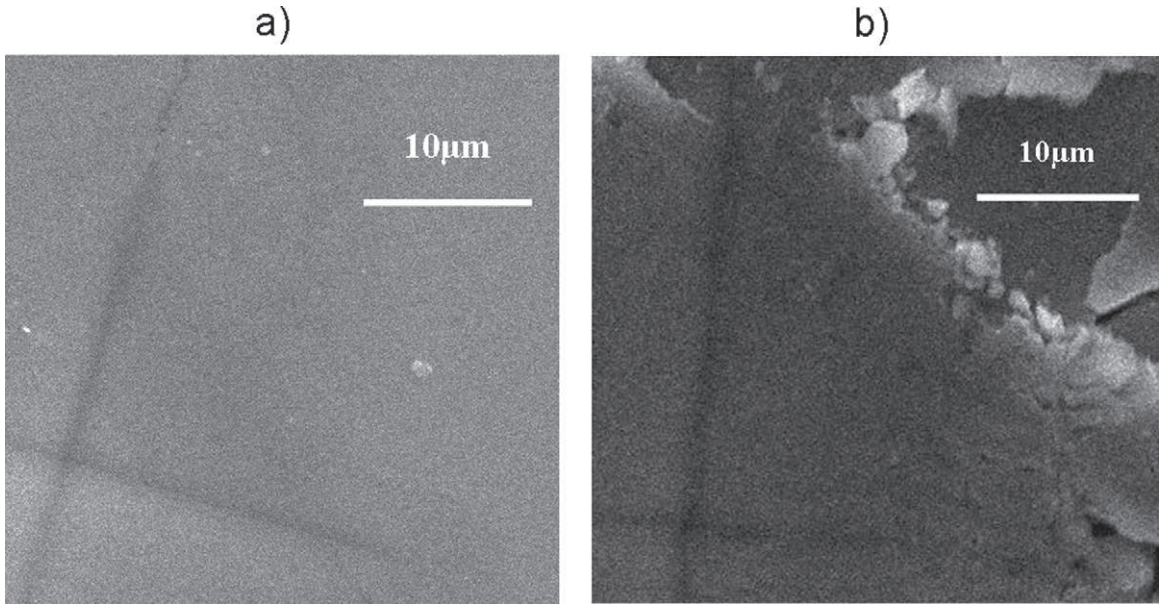

Fig. 12. Micrographs obtained by SEM on sample surfaces after indentation at 9.8N load (a) in the zones with small grains (b) in the zones with large grains.

larger in diagonal than in the zone with small grains. Moreover, broken parts of large grains are observed in Fig. 12, by SEM micrographic analysis at the edge of the indentation.

This tendency of large grains to be taken off the matrix is also supported by surface roughness measurements after polishing of the samples. Whereas parts with small grains are smooth with a peak-to-valley height of 0.4 μm, a residual roughness after polishing is measured on the zones with large grains with a peak-to-valley value of 10 μm (which is the average size of large grains). Moreover, the skewness of the roughness profile is negative with values from −1 to −3. These large negative values are typical of asymmetrical roughness profiles with preponderance of holes as compared to hills (the bulk of the material being above the mean line).

Hence, lack of cohesion between the large grains could be the limiting parameter to lithium migration and the explanation of the lower total ionic conductivity of the pellets sintered at 1000 °C. For the other pellets, the presence of zones with large grains is not detrimental to the global conductivity. We can then infer that in these cases the zones with small grains promote the mechanical cohesion between the large particles.

6. Conclusion

Powders with high purity have been prepared by co-precipitation method. LATP pellets sintered by Spark Plasma Sintering with conductivities amongst the highest published are obtained with 1.6×10^{-4} S/cm at room temperature. Very high densities are also obtained (97% of the theoretical density) so that these membranes can be readily used as separator for aqueous lithium-air batteries. Moreover, these dense and conductive pellets were synthesized at temperatures as low as 850 °C and for treatment duration of 5 min whereas by classical sintering at temperature of 1000 °C for 1 h would be necessary. A new feature that could be brought to the knowledge of the research field is the correlation of the drop in conductivity with the loss of cohesion of grains as SPS sintering temperature reaches 1000 °C. Investigations are going on to determine the origin of this phenomenon, where the presence of amorphous phases at the grain boundaries is being hypothesized.

Acknowledgements

This work was supported by the French National Research Agency (project ANR LiO_2). The SPS sintering was performed at the SPS French National Platform (PNF2/CNRS) at Toulouse. We especially thank Geoffroy Chevallier and Claude Estournes for their technical support.

References

1. Tarascon JM, Armand M. Issues and challenges facing rechargeable lithium batteries. *Nature* 2001;**414**:359–67.
2. Armand M, Tarascon JM. Building better batteries. *Nature* 2008;**451**:652–7.
3. Visco SJ, Nimon E, De Jonghe LC. Secondary batteries: metal-air systems | lithium-air. In: Jürgen G, editor. *Encyclopedia of electrochemical power sources*. Amsterdam: Elsevier; 2009. p. 376–83.
4. Ji DX, Tae LK, Nazar LF. *Challenges of lithium-sulfur and lithium-air cells: old chemistry, new advances. On: scalable energy storage: beyond lithium-ion.* San Jose, USA: Almaden Institute; 2009. Aug. 26.
5. Bruce PG, Freunberger SA, Hardwick LJ, Tarascon J-M. LiO_2 and LiS batteries with high energy storage. *Nat Mater* 2012;**11**:19–29.
6. Visco, S., Nimon, Y., inventors; PolyPlus Battery Company, assignee. Li/Air non aqueous batteries. United States patent US 20070117007. 2007 May 24.
7. Stevens, P., Toussaint, G., inventors; Electricité de France, assignee. Dispositif électrochimique à électrolyte solide conducteur d'ions alcalins et à électrolyte aqueux. WO 2011051597. 2011 May 5.
8. Abraham KM, Jiang Z. A polymer electrolyte-based rechargeable lithium/oxygen battery. *J Electrochem Soc* 1996;**143**:1–5.
9. Ogasawara T, Debart A, Holzapfel M, Novak P, Bruce PG. Rechargeable Li_2O_2 electrode for lithium batteries. *J Am Chem Soc* 2006;**128**:1390–3.

10. Kumar B, Kumar J, Leese R, Fellner JP, Rodrigues SJ, Abraham KM. A solid-state, rechargeable, long cycle life lithium-air battery. *J Electrochem Soc* 2010;**157**:A50–4.
11. Lapp T, Skaarup S, Hooper A. Ionic conductivity of pure and doped Li_3N. *Solid State Ionics* 1983;**11**:97–103.
12. Bruce PG, West AR. The AC conductivity of polycrystalline Lisicon $Li_{2+2x}Zn_{1-x}GeO_4$, and a model for intergranular constriction resistances. *J Electrochem Soc* 1983;**130**:662–9.
13. Aono H, Sugimoto E, Sadaoka Y, Imanaka N, Adachi G. Ionic conductivity of solid electrolytes based on lithium titanium phosphate. *J Electrochem Soc* 1990;**137**:1023–7.
14. West WC, Whitacre JF, Lim JR. Chemical stability enhancement of lithium conducting solid electrolyte plates using sputtered LiPON thin films. *J Power Sources* 2004;**126**:134–8.
15. Fu J. Superionic conductivity of glass-ceramics in the system Li_2O–Al_2O_3–TiO_2–P_2O_5. *Solid State Ionics* 1997;**96**:195–200.
16. Arbi K, Mandal S, Rojo JM, Sanz J. Dependence of ionic conductivity on composition of fast ionic conductors $Li_{1+x}Ti_{2-x}Al_x(PO_4)_3$, $0 \leq x \leq 0.7$. A parallel NMR and electric impedance study. *Chem Mater* 2002;**14**:1091–7.
17. Cretin M, Fabry P. Comparative study of lithium ion conductors in the system $Li_{1-x}Al_xA^{IV}{}_{2-x}(PO_4)_3$ with A^{IV} = Ti or Ge and $0 \leq x \leq 0.7$ for use as Li^+ sensitive membranes. *J Eur Ceram Soc* 1999;**19**:2931–40.
18. Aatiq A, Menetrier M, Croguennec L, Suard E, Delmas C. On the structure of $Li_3Ti_2(PO_4)_3$. *J Mater Chem* 2002;**12**:2971–8.
19. Nuspl G, Takeuchi T, Weiss A, Kageyama H, Yoshizawa K, Yamabe T. Lithium ion migration pathways in $LiTi_2(PO_4)_3$ and related materials. *J Appl Phys* 1999;**86**:5484–90.
20. Barj M, Perthuis H, Colomban P. Existence domains, structural distortions and vibration modes of conducting ions in Nasicon host lattices. *Solid State Ionics* 1983;**11**:157–77.
21. Martinez-Juarez A, Pecharroman C, Iglesias JE, Rojo JM. Relationship between activation energy and bottleneck size for Li + ion conduction in NASICON materials of composition $LiMM'(PO_4)_3$; M, M ′ = Ge, Ti, Sn, Hf. *J Phys Chem B* 1998;**102**:372–5.
22. Aono H, Sugimoto E, Sadaoka Y, Imanaka N, Adachi G. Ionic conductivity and sinterability of lithium titanium phosphate system. *Solid State Ionics* 1990;**40–1**:38–42.
23. Randles JEB. Kinetics of rapid electrode reactions. *Discuss Faraday Soc* 1947;**1**:11–9.
24. Ando Y, Hirose N, Kuwano J, Kato M, Otsuka H. *Ceramics today-tomorrow's ceramics*. Amsterdam: Elsevier; 1991.
25. Louchet F, Weiss J, Richeton T. Hall–Petch law revisited in terms of collective dislocation dynamics. *Phys Rev Lett* 2006;**97**, 075504-1-4.